Effect of Ionic Liquid 1-Butyl-3-Methylimidazolium Bis(Trifluoromethanesulfonyl)Imide on the Properties of Poly(Glycidyl Methacrylate) Based Solid Polymer Electrolytes[1]

M. R. N. Nabilah[a], M. A. Alwi[a], M. S. Su'ait[b], M. Imperiyka[c], S. A. Hanifah[a], A. Ahmad[a, b], N. H. Hassan[a, *], and M. Y. A. Rahman[d, **]

[a]*School of Chemical Sciences and Food Technology, Faculty of Science and Technology, University Kebangsaan Malaysia, 43600, Bangi, Selangor, Malaysia*

[b]*Solar Energy Research Institute (SERI), University Kebangsaan Malaysia, 43600, Bangi, Selangor, Malaysia*

[c]*Faculty of Arts and Sciences, Kufra Campus, University of Benghazi, Al Kufrah, Libya*

[d]*Institute of Microengineering and Nanoelectronics (IMEN), University Kebangsaan Malaysia, 43600, Bangi, Selangor, Malaysia*

*e-mail: syareeda@ukm.edu.my

**e-mail: mohd.yusri@ukm.edu.my

Received May 20, 2015

Abstract—A free standing polymer electrolytes films, containing poly(glycidyl methacrylate) (PGMA) as the polymer host, lithium perchlorate (LiClO$_4$), and ionic liquid 1-butyl-3-methylimidazolium bis(trifluoromethanesulfonyl)imide [Bmim][TFSI] as a plasticizer was successfully prepared via the solution casting method. The XRD analysis revealed the amorphous nature of the electrolyte. ATR-FTIR and thermal studies confirmed the interaction and complexation between the polymer host and the ionic liquid. The maximum ionic conductivity of the solid polymer electrolyte was found at 2.56×10^{-5} S cm^{-1} by the addition of 60 wt % [Bmim][TFSI] at room temperature and increased up to 3.19×10^{-4} S cm^{-1} at 373 K, as well as exhibited a transition of temperature dependence of conductivity: Arrhenius-like behavior at low and high temperatures.

1. INTRODUCTION

Solid polymer electrolytes (SPEs) are gaining more attention nowadays as a promising candidate to replace the usage of toxic, hazardous, and leakable liquid electrolyte in electrochemical devices. SPEs are generally defined as polymeric materials complexed with metal salts and widely used in electrochemical devices application such as batteries, solar cells, sensors, capacitors and fuel cells as ionic medium for charge carriers as well as conductive separators [1]. It is an attractive material because of its special properties, such as easy of handling and manufacturing process, light weight, can be operated at high temperature, high automation potential, no separator needed and multifunctional cell design flexibility of SPE [2–4].

Recently, acrylate based polymer electrolyte received a lot of attention due to its feasible and fast curing properties obtained by photo-polymerization technique. Photo-polymerization is very attractive technique because it is a very rapid reaction, simple method, and cost effective, which is an important factor in large scale production [5–7]. One of the outstanding acrylate based polymer electrolyte is polyglycidyl methacrylate (PGMA), which is a class of ester which consists of functional groups of ether, carbonyl, and epoxy ring. The polarity of these functional groups provides an active site for ions to form coordination [5, 8]. It has received more attention due to its low toxicity in both monomer and polymer forms, and having excellent flexibility, thermal, and mechanical stability compared to others methacrylate compounds [5]. Imperiyka et al. [9] reported that the highest conductivity of PGMA–LiClO$_4$ was obtained upon the addition of 30 wt % LiClO$_4$ with the value of 4.2×10^{-5} S cm^{-1}. The ionic conductivity value was found to be reduced after the addition of lithium salt at 30 wt % and more. With the aims to raise the ionic conductivity value by increasing the ionic mobilities, acrylate based polymer electrolytes were designed with inclusion of room temperature ionic liquids (RTILs)

---

[1] The article is published in the original.

into the electrolytes system. RTILs, which are also known as molten salts, have become prominent materials in SPE due to their unique properties such as non-volatile, non-toxic and non-flammable qualities. They consist of bulky organic cations and highly delocalized-charge inorganic anions, along with low melting point (<100°C) [10]. Moreover, RTILs acts as a plasticizer in the SPE system, which improved the movement of polymeric chains, therefore provide free volume for ions transportations [11]. These properties are expected to enhance ion dissociation of lithium salts, thus contributed for high ionic conductivity. Based on earlier study, doping ionic liquid into polymeric system enhances and generates ionic conductivity up to ~10^{-5} S cm^{-1} [12–14].

PGMA–LiClO$_4$–BmimTFSI based polymer electrolyte film was prepared via solution casting technique and characterized using scanning electron microscopy (SEM), X-ray diffraction (XRD), Fourier transformation infra-red spectroscopy (ATR-FTIR) AC electrochemical impedance spectroscopy (EIS), differential scanning calorimetry (DSC), and thermogravimetry analysis (TGA) to observe the effect of BmimTFSI weight percentages on the morphology, structure, chemical interaction, ionic conductivity and thermal properties of the electrolyte. It is expected that the ionic conductivity value will rise along with the increase of RTILs weight percentages and remained their flexibility and thermal stability properties.

2. EXPERIMENTAL DETAILS

2.1. Material

Glycidyl methacrylate (GMA) with an average molecular weight of 142.15 g mol^{-1} (Aldrich), lithium perchlorate (LiClO$_4$) (Aldrich), dichloromethane (DCM) (J.T. Baker), 2,2-dimethoxy-2-phenylacetophenone (DMPP) (Aldrich) and tetrahydrofuran (THF) (J.T. Baker) were used without further purification, except for the ionic liquid 1-butyl-3-methylimidazolium bis(trifluoromethanesulfonyl)imide (BmimTFSI) (Merck).

2.2. Purifying the BmimTFSI

BmimTFSI ionic liquid was mixed in DCM and this combined organic system was rinsed with a small amount of the deionized water until the aqueous phase was halide free (silver nitrate test). DCM was removed through evaporation process inside a fume chamber. The ionic liquid was finally stored under nitrogen gas.

2.3. Preparation of SPE

The synthesis of the PGMA is according to the previous method [9]. 2,2-Dimetoxy-2-phenylacetophenon (DMPP), as photo-initiator was mixed into an appropriate amount of GMA. The mixture was exposed to the UV radiation in UV box (Rs. Ltd.) containing four 60 W UV lamps under continuous flow of nitrogen gas for 5–10 min. After the polymerization was completed, the homopolymer was rinsed with methanol to remove any impurities or unreacted monomer. The homogenous solutions of PGMA with different concentrations of ionic liquid were prepared via solution casting method. 3 g of the PGMA was added into the 30 mL of THF and stirred for 24 h. The amount of LiClO$_4$ were fixed at 30 wt % and various weight percentages of BmimTFSI ionic liquid were dissolved separately in different Erlenmeyer flask with half amount of THF (15 mL) for 12 h. These three separate solutions were mixed and further stirred for 24 h. The homogenous electrolyte solution was then poured onto a teflon mould and the solvent was allowed to evaporate slowly at room temperature. The electrolyte film was further dried in a vacuum oven at 55°C for 72 h in order to remove any residual solvent. The free standing film was peeled off from the mould and stored in a dry box for further characterization.

2.4. Characterization

The morphological observation on the polymer electrolyte films was observed by scanning electron microscopy model Philips CM 12 and examined at 15 kV with <10^3 K magnification at room temperature. The samples were coated with thin layer of gold in order to make them more conductive, resulting clear micrograph. The structure of the electrolyte was investigated via X-ray diffractometer (XRD) model Bruker D8-Advance diffractometer within the range between $2\theta = 3°–70°$. Attenuated total reflectant-Fourier transform infrared (ATR-FTIR) analysis was carried out by using spectrometer Perkin Elmer Spectrum 2000 from 4000 to 650 cm^{-1} with scan resolution of 2 cm^{-1}. It was used to investigate the interaction between the PGMA-salt complexes with the BmimTFSI ionic liquid. The ionic conductivity was analyzed using HIOKI-3532-50 LCR HiTESTER at the frequency range between 50 Hz–5 MHz at ambient temperature, as well as temperature up to 100°C, for temperature dependence on conductivity. The conductivity of the sample was calculated using Eq. (1),

$$\sigma = I/R_b A, \qquad (1)$$

I is the film thickness (0.02–0.03 cm), R_b is the bulk resistance determined from the complex impedance plot and A is the contact area between the electrolyte and the electrode (cm^2). The thickness of the sample was measured using a digital calliper (Mitotuya).

The $[O/(Li^+ + Bmim^+)]$ ratio for a single polymer was calculated by extending the equation into binary charge carriers system (2) [5]:

$$\left[O/(Li^+ + Bmim^+)\right]$$
$$= \frac{M_{PGMA} \times (M_{W\,LiClO_4} + M_{W\,BmimTFSI}) \times n_{PGMA}}{(M_{LiClO_4} + M_{BmimTFSI}) \times M_{W\,PGMA}}, \quad (2)$$

where M_{PGMA} = mass of PGMA (g), $M_{W\,LiClO4}$ = molecular weight of LiClO$_4$ salt (g mol^{-1}), $M_{W\,BmimTFSI}$ = molecular weight of BmimTFSI (g mol^{-1}), M_{LiClO4} = mass of LiClO$_4$ salt (g), $M_{BmimTFSI}$ = mass of BmimTFSI (g), $M_{W\,PGMA}$ = molecular weight of PGMA (g mol^{-1}), n_{PGMA} = number of oxygen atom in PGMA per repeated unit monomer.

DSC was used to study the glass transition temperature (T_g) of PGMA–LiClO$_4$ and PGMA–LiClO$_4$–BmimTFSI in the temperature range from 20 to 170°C at 10°C/min. Thermogravimetry analysis was measured from room temperature up to 600°C. Both analyses were performed under dynamic nitrogen gas with Setaram Instrument DSC/TGA analyzer model Labsys Evo.

## 3. RESULTS AND DISCUSSION

3.1. Morphological Observation

Figure 1 illustrates morphological observation for (a) PGMA and PGMA–LiClO$_4$, with (b) 0 wt %, (c) 20 wt %, (d) 60 wt % and with (e) 70 wt % BmimTFSI. Figure 1a represents the morphological observation of porous structure that might be due to the evaporation of solvent during the casting process in pure polymer host, PGMA [15]. Figure 1b shows PGMA polymer matrix with the inclusion of lithium salt, whereby the salt is indicated to dissolve in the polymer matrix as no trace of salt's crystals is observed [5]. Similar to Fig. 1a, the observed pinholes is believed was due to the evaporation of solvent during the casting process. After the addition of ionic liquid BmimTFSI into the polymer matrix, a smoother and homogenous surface was produced on the fracture samples up to 60 wt % BmimTFSI with ordered strips that showed arrangements of polymer and BmimTFSI in the system. This may a consequence of entrapment of BmimTFSI in the polymer matrix [16]. According to literatures, the appearance of the smooth surface on SEM micrograph is strongly related to amorphous nature of polymer [5, 7, 8, 15, 17]. Leones et al. [15] indicated the increase in amorphous nature of SPE increases the flexibility of the polymer backbone, thus facilitates ion mobility through the polymer system, and increases the ionic conductivity of the SPE [15]. The morphology of PGMA–LiClO$_4$–BmimTFSI SPE became rough after further addition of 70 wt % BmimTFSI, as observed in Fig. 1e.

3.2. Structural Studies

The respective diffraction patterns of pure PGMA, and PGMA–LiClO$_4$ with various wt % of BmimTFSI are shown in Fig. 2. The polymer host, PGMA, shows semi-crystalline characteristics between Bragg angle of $2\theta = 5°$ to $18°$. From the diffraction pattern, it obviously shows that upon the addition of BmimTFSI, the semi-crystalline intensities are reduced significantly. The reduction in the intensity of the semi-crystalline peak also indicates the amorphous characteristic of the polymer electrolyte increases [18]. It is believed that the arrangement order of polymer matrix has been distracted by addition of BmimTFSI ionic liquid, as a result it has decreased the crystallinity region and rigidity of the polymer backbone [12, 19]. According to the previous report [5], higher amorphous region in polymer matrix provide more free volume for the segmental motion, thus accelerates the ionic mobility, and thereby, increases the ionic conductivity significantly. After the addition of 70 wt % BmimTFSI, the intense crystallization peaks are apparently observed at $2\theta = 13°$, $23°$, $26°$, $35°$ and $56°$, which correspond to those of LiClO$_4$ which is at $2\theta = 12°$ to $13°$, $20°$ to $22°$, $22°$ to $24°$, $31°$ to $32°$, 32 to $33°$ and $57°$. The existence of intense crystallization peak shows ion association and coagulation to lead the decrease in conductivity.

3.3. Thermal Studies

Figure 3 illustrates the DSC curves for PGMA, PGMA–LiClO$_4$ and PGMA–LiClO$_4$–60 wt % BmimTFSI SPE. The experimental glass transition for pristine PGMA is at 43°C. There is an increase of T_g value for PGMA–LiClO$_4$, which is 97°C and this values decreased after the presence of 60 wt % BmimTFSI to 41°C. The plasticizing behaviour of ionic liquid [20] is believed as the major effect that reduces the glass transition temperature of PGMA–LiClO$_4$–60 wt % BmimTFSI SPE. BmimTFSI helps to reduce the crystallinity of the polymer matrix by destroying the ordered arrangement of the polymer backbone [6]. The plasticizer softens the polymer backbone. The increase in amorphous region enhances the flexibility of the polymer that results in the acceleration of polymer segmental motion and thus, provides more void and free space for ion migration and thereby, increases the ionic conductivity by providing more conducting pathways [13, 14]. According to Ramesh et al. [16], the existence of BmimTFSI in polymer electrolyte system weakens the dipole-dipole interactions between polymer chain and reduces the solvation effect of Li$^+$ cation, thus disrupts the cross linking bonds among the polymer matrix. This contributes in promoting the ion coupling due to its high self-dissociating, as well as ionic hopping properties, and subsequently, enhances ionic mobility towards high ionic conductivity [12].

(a)

(b)

20 μm

2 μm

(c)

(d)

2 μm

2 μm

(e)

2 μm
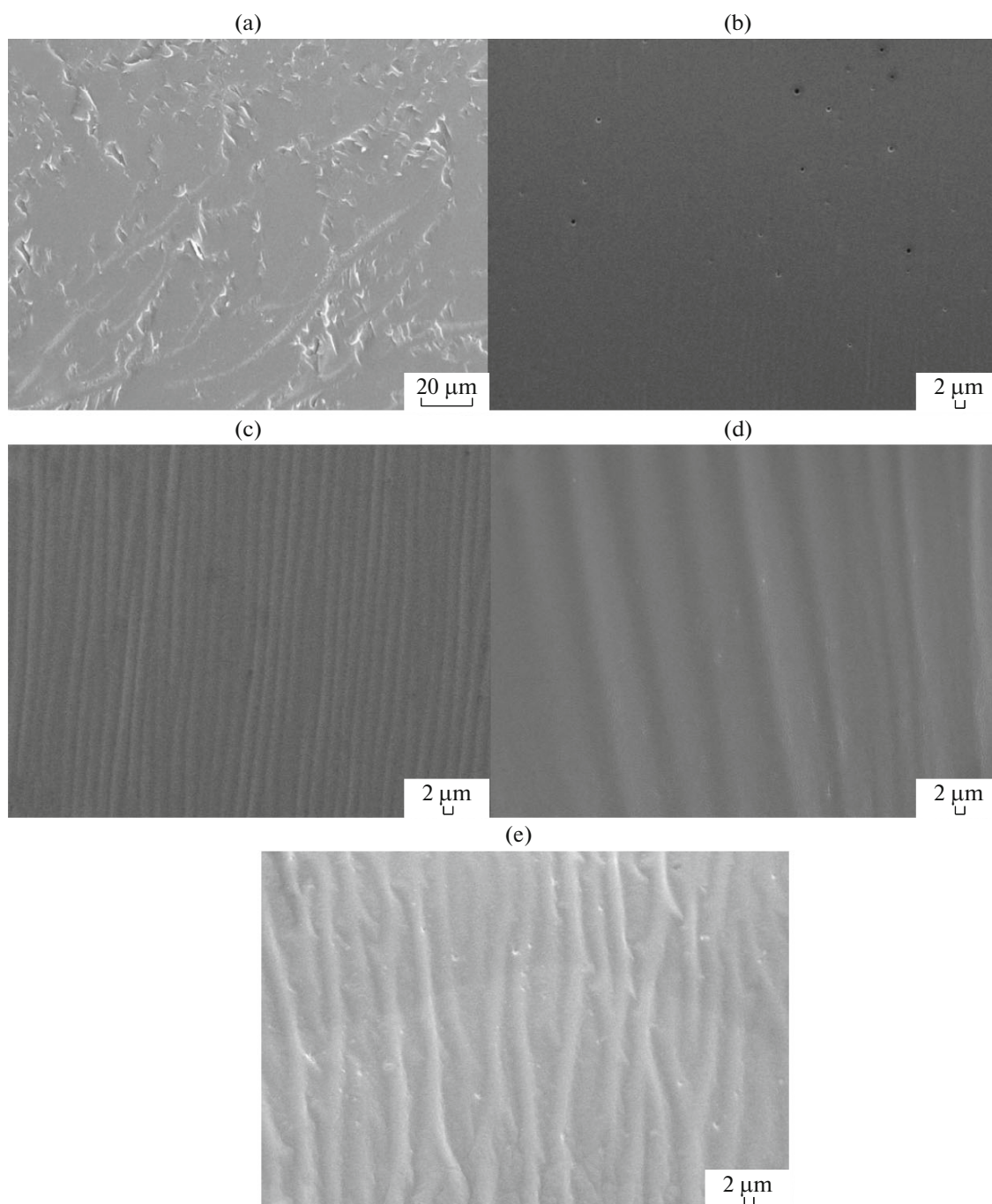
Fig. 1. SEM images for (a) PGMA and PGMA–LiClO$_4$ with (b) 0 wt %, (c) 20 wt %, (d) 60 wt %, and (e) 70 wt % BmimTFSI.

Figure 4 shows TGA thermograms of pristine PGMA, classic polymer electrolytes PGMA–LiClO$_4$, and PGMA–LiClO$_4$, with the inclusion of 60 wt % BmimTFSI, while Table 1 indicates the weight loss (wt %) of PGMA, PGMA–LiClO$_4$, and PGMA–LiClO$_4$–60 wt % BmimTFSI. The thermograms show single step thermal degradation (T_d) of pristine PGMA, PGMA–LiClO$_4$, and PGMA–LiClO$_4$–60 wt % BmimTFSI. The first thermal degradation (T_{d1}) stage of PGMA in Fig. 4 is observed at 284°C with 10 wt % loss and achieves its temperature at maximum weight loss (T_{max}) at second thermal degradation (T_{d2}) at 298°C with the highest yield up to 51 wt % loss. The T_{d1} degradation starts with the depolymerization of the unsaturated chain ends to monomers, followed by random decomposition of ester chain scission at the T_{d2}, which results in elimination of acrolein, allyl alcohol, carbon monoxide, carbon dioxide,
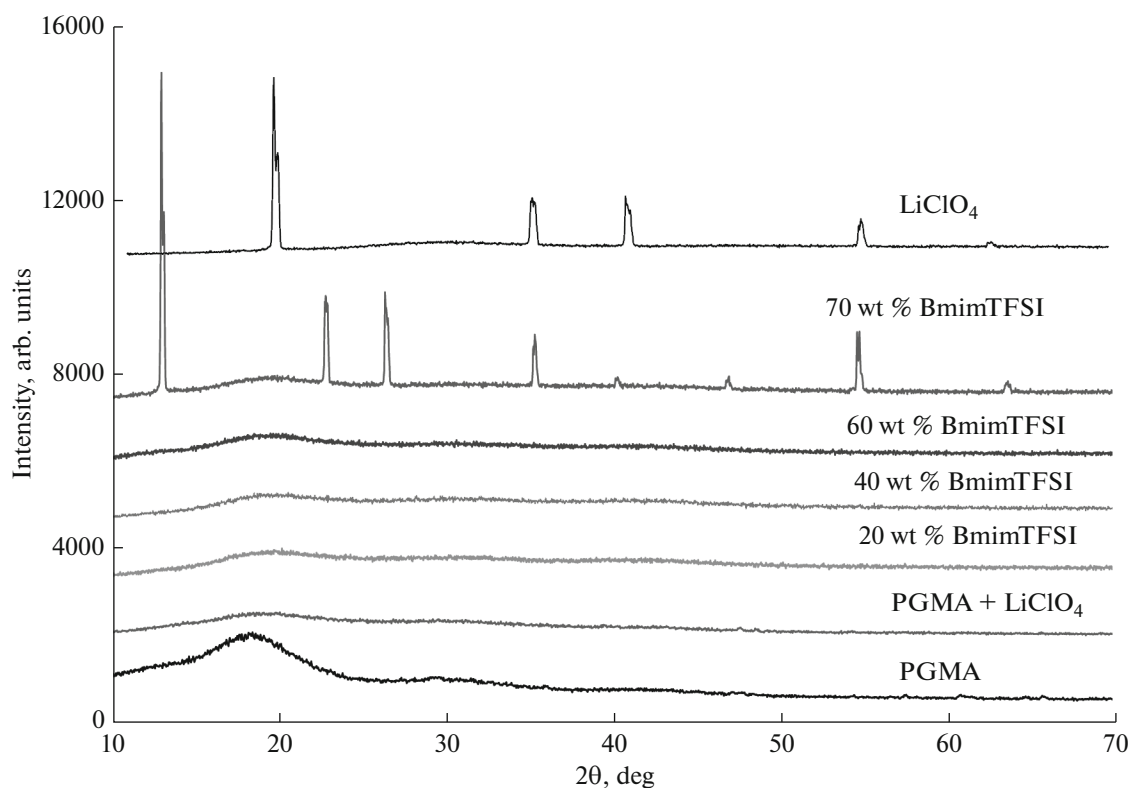
Fig. 2. XRD pattern for PGMA−LiClO₄−BmimTFSI solid polymer electrolyte.

dimethyl ketene, isobutene, propene and glycidol [21−32]. The third thermal degradation (T_{d3}) stage is observed at 429°C with 21 wt % loss and 18 wt % of residue left after thermal decomposition that took place up to 600°C. The T_{d3} decomposition is related to the decomposition of minor products arising from ester decomposition such as acrolein, allyl alcohol, glycidol, isobutene, and propene to form gasses products such as carbon dioxide and carbon monoxide [30].
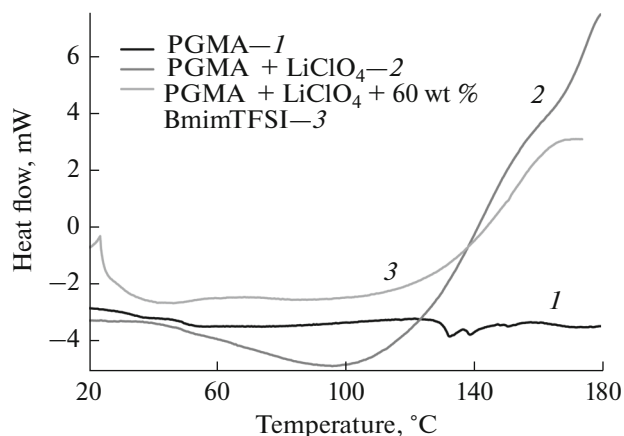

Fig. 3. DSC thermograms of (*1*) PGMA, (*2*) PGMA−LiClO₄ and (*3*) PGMA−LiClO₄−BmimTFSI.

With the presence of LiClO₄ in PGMA, a slight weight loss was observed in the region of 23−214°C in Fig. 4 is mainly related to the vaporization of moisture and solvent residue due to hydroscopic nature of LiClO₄ salt. The T_{d2} of thermal degradation is found to increase to 324°C and further increased to 346°C with the highest yields of weight loss at 62 wt % after the introduction of BmimTFSI into the PGMA−LiClO₄ system. The increase in T_d of PGMA−LiClO₄ after the addition of BmimTFSI ionic liquid indicates higher thermal stability of polymer electrolytes. The ionic liquid is believed to form a strong intermolecular interaction between the cation and the (C−O−C) polymeric segment, as supported by the FTIR analysis. The strong interaction requires more heat to break the PGMA−LiClO₄−BmimTFSI polymer electrolytes. This phenomenon results in higher thermal stability of polymer electrolytes as demonstrated in the TGA thermograms [33].

3.4. Infrared Analysis

The vibrational mode for the various types of functional groups in PGMA based on polymer electrolyte is analyzed from Fig. 5 and Fig. 6 and summarized in Table 2. The main focus of this investigation is the region of carbonyl functional group (C=O) (1850−1650 cm⁻¹), ether (C−O−C) (1300−1000 cm⁻¹) and
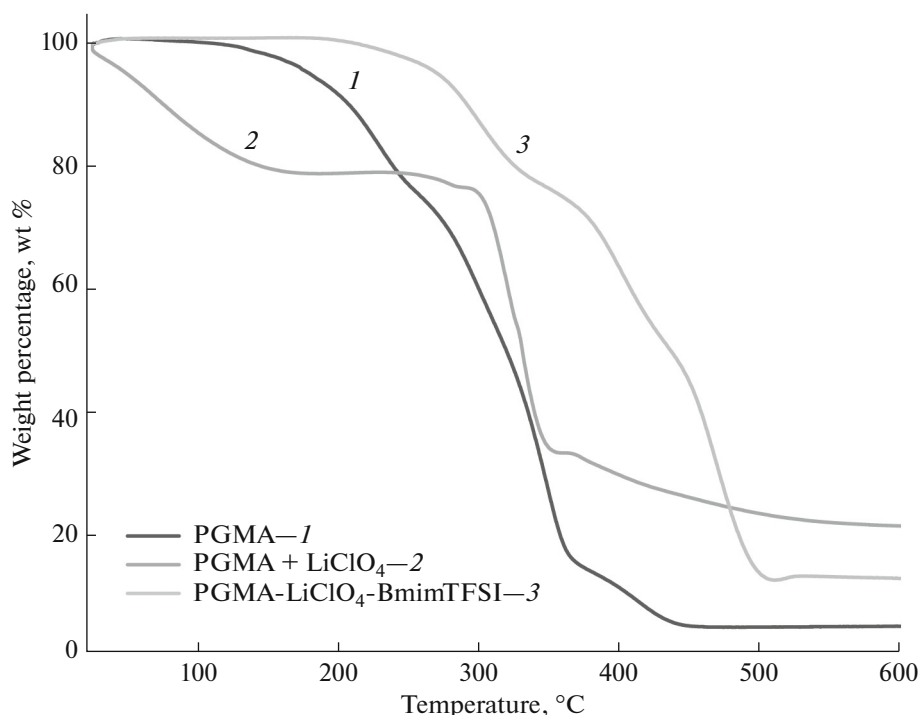
Fig. 4. TGA thermograms of (*1*) PGMA, (*2*) PGMA–LiClO$_4$ and (*3*) PGMA–LiClO$_4$–BmimTFSI.

epoxy (C–O–C) (1280–1230, 950–815 and 880–750 cm^{-1}) group in PGMA. It is also interesting to observe the effect of the interaction on amine active site and neighbouring functional group in BmimTFSI ionic liquid.

Figure 5 illustrates the FTIR spectra for carbonyl functional group (C=O) of PGMA homopolymer, and PGMA–LiClO$_4$ with 0, 20, 40, 60 wt % BmimTFSI. Carbonyl stretching mode of ester in PGMA homo-polymer is observed at 1718 cm^{-1} and is shifted to 1716 cm^{-1} upon the addition of 40 to 60 wt % of BmimTFSI. Lower wavenumber in carbonyl stretching mode of ester is due to the appearances of conjugated C=C stretching from PGMA monomers, as observed at 1643 and 998 cm^{-1} (*cis* and *trans* stretching mode, respectively).

Figure 6 shows FTIR spectrum for ether functional group (C–O–C) of PGMA homo-polymer, and PGMA–LiClO$_4$ with 0, 20, 40, 60 wt % BmimTFSI.

The ether asymmetric and symmetric stretching modes in PGMA are examined at 1153 and 1072 cm^{-1}. The inclusion of BmimTFSI has shifted the (C–O–C) asymmetric stretching mode to 1132 cm^{-1} and symmetric mode to 1095 cm^{-1}. While, the change is insignificant at 848 and 905 cm^{-1} for (C–O–C) symmetric and asymmetric stretching of epoxide ring in PGMA. It is also revealed that C–O–C weak ring stretching bend (breathing mode) of epoxide ring in PGMA, observed at 1256 cm^{-1}, is shifted to 1230 cm^{-1}. The shift indicates that there is a strong interaction at oxygen lone pairs of ether and epoxide ring in PGMA.

The SO$_2$ asymmetric stretching, CF$_3$ symmetric stretching, and bending of bis(trifluoromethyl)sulfonyl-imide [TFSI]$^-$ from BmimTFSI ionic liquid are shown at 1350, 1196, 1139, and 761 cm^{-1}, respectively. The CF$_3$ symmetric stretching of [TFSI]$^-$ is shifted to 1187–1183 cm^{-1}. While, CF$_3$ bending of [TFSI]$^-$ in

Table 1. Percentage of weight loss (wt %) of PGMA, PGMA–LiClO$_4$, and PGMA–LiClO$_4$–60 wt % BmimTFSI

Sample (NCO/OH)	% Weight loss (wt %)			Total Weight loss (wt %)	Residue after 600°C (%)
	T_{d1} (~280°C)	T_{d2} (~300°C)	T_{d3} (~430°C)		
PGMA	10	51	21	82	18
PGMA–LiClO$_4$	21	44	12	77	23
PGMA–LiClO$_4$–BmimTFSI	26	62	9	97	3
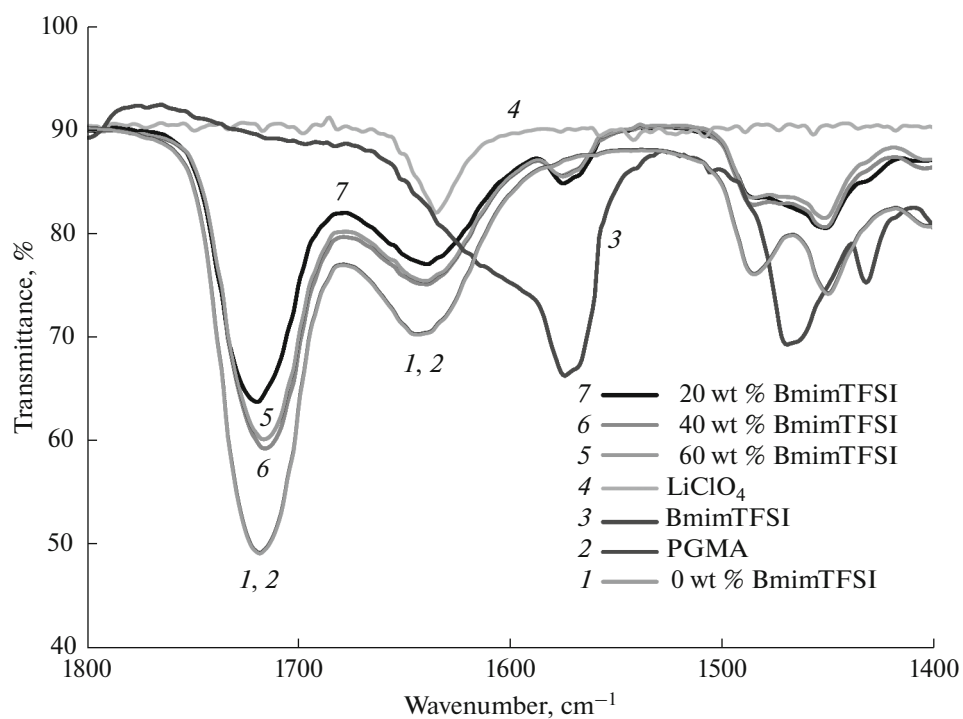
Fig. 5. FTIR spectra for carbonyl functional group (C=O) of PGMA homo-polymer and PGMA–LiClO₄ with 0, 20, 40, 60 wt % BmimTFSI, pure BmimTFSI and LiClO₄, as references.
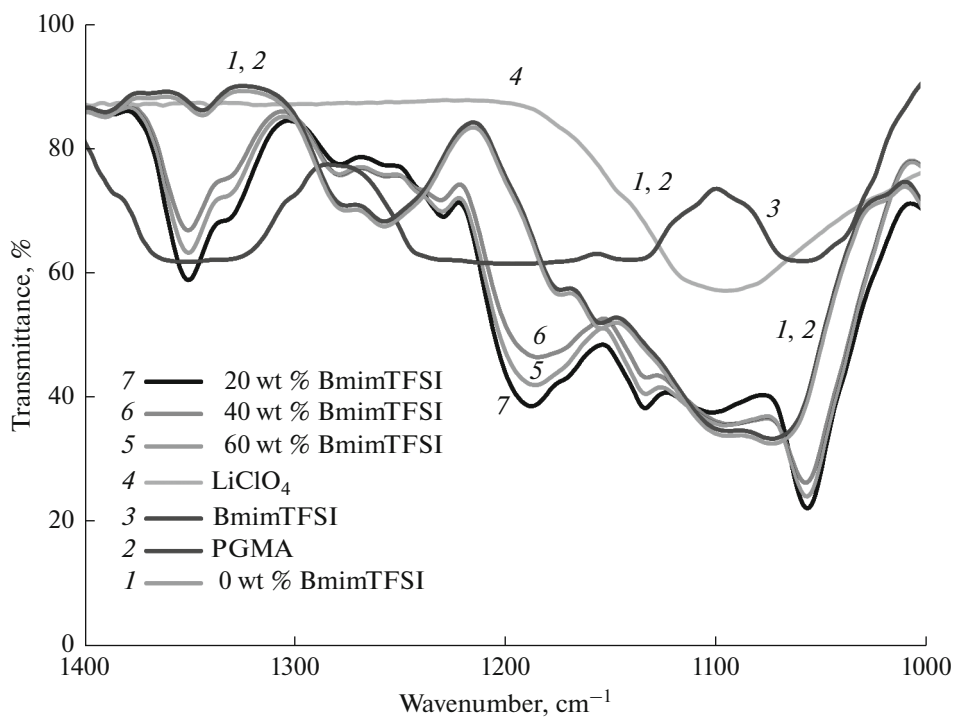
Fig. 6. FTIR spectra for ether functional group (C–O–C) region of PGMA homo-polymer and PGMA–LiClO₄ with 0, 20, 40, 60 wt % BmimTFSI.

Table 2. Vibrational mode for the various types of functional groups (cm^{-1}) in PGMA–LiClO$_4$–BmimTFSI SPEs

Description of vibrational mode	PGMA	BmimTFSI	0 wt % BmimTFSI	20 wt % BmimTFSI	40 wt % BmimTFSI	60 wt % BmimTFSI
CF$_3$ symmetric stretching and bending [TFSI]$^-$	—	1196, 1139, 761	—	1187	1183	1184
SO$_2$ asymmetric stretching	—	1350	—	1350	1350	1350
N–H stretching & out-of-plane bending of Bmim$^+$	—	790	—	1228, 791	1230, 791	1229, 791
CH$_2$ scissoring and rocking	1485, 749	1469, 741	1485, 749	1484, 743	1485, 747	1485, 747
CH$_3$ asymmetric bending	1450	1432	1450	1451	1452	1452
–CH$_2$ stretching (sp^3)	2942, 2930	2968, 2941, 2881	2930, 2930	2965, 2940, 2882	2964, 2946, 2883	2963, 2946, 2882
–C–H antisymmetric & symmetric stretching (sp^2)	3005	3158, 3122	3005	3167, 3138	3167, 3138	3167, 3138
C=C stretching of Bmim$^+$	—	1574,	—	1575	1576	1575
C–N stretching of Bmim$^+$	—	1057		1055	1056	1055
C=O stretching in PGMA	1718	—	1718	1718	1716	1716
C=C *cis* and *trans* stretching	1643, 988	—	1643, 988	1639, 991	1639, 990	1642, 990
C–O–C ether stretching in PGMA	1153, 1072	—	1153, 1072	1132, 1100	1131, 1092	1132, 1095
C–O–C asymmetric & symmetric epoxide ring in PGMA	905, 848	—	905, 848	907, 846	906, 848	907, 846
C–O–C weak ring stretching bend (breathing mode) of epoxide ring in PGMA	1256	—	1256	1228	1229	1230

Table 3. Variation of room temperature ionic conductivity and $[O/(Li^+ + Bmim^+)]$ ratio of PGMA–LiClO$_4$ at different wt % of ionic liquid BmimTFSI

Wt % [Bmim][TFSI]	Ionic conductivity, σ (S cm^{-1})	$[O/(Li^+ + Bmim^+)]$ ratio
0	2.27×10^{-7}	7/1
10	1.98×10^{-6}	28/1
20	2.55×10^{-6}	22/1
30	2.71×10^{-6}	19/1
40	3.12×10^{-6}	16/1
50	1.42×10^{-5}	14/1
60	2.56×10^{-5}	12/1
70	8.23×10^{-6}	11/1

PGMA based BmimTFSI polymer electrolytes overlaps with CH$_2$ rocking of PGMA (749 cm^{-1}) and [Bmim]$^+$ (741 cm^{-1}) to 747–743 cm^{-1}. The CH$_2$ scissoring and CH$_3$ asymmetric bending of PGMA, N−H bending mode (out-of-plane), C=C (overlaps with N−H bending—primary amine), and C−N stretching of Bmim$^+$ are not distorted with the addition of BmimTFSI. However, −CH$_2$ stretching (sp^3) of [Bmim]$^+$ (2968, 2941, 2881 cm^{-1}) are shifted to 2963, 2946, 2882 cm^{-1}. Besides, −C−H antisymmetric and symmetric stretching (sp^2) of cyclic Bmim$^+$ (3158, 3122 cm^{-1}) are shifted to 3167, and 3138 cm^{-1}. The C−H vibrational mode for cyclic Bmim$^+$ suggests interactive bond with oxygen group from PGMA. More importantly, the appearance of N−H stretching mode of primary amine in Bmim$^+$ is observed at 1228 cm^{-1}. This indicates the interaction between the oxygen lone pairs of ether and epoxide ring in PGMA with Bmim$^+$ weakens the bond between BmimTFSI, which accelerates the ion dissociation and leads to ion transportation by the formation of polymer-BmimTFSI complex [12, 19]. As a result, more mobile carriers are produced and led to higher ionic conductivity. These results are in agreement with the conductivity measurement.

3.5. Ionic Conductivity Studies

The relationship between ionic conductivity and $[O/(Li^+ + Bmim^+)]$ ratio at different concentration of ionic liquid BmimTFSI at room temperature is shown in Table 3. The ionic conductivity of PGMA–LiClO$_4$–BmimTFSI is found to increase with the addition of BmimTFSI concentration. The highest room temperature ionic conductivity was obtained at 60 wt % of BmimTFSI with the value of 2.56×10^{-5} S cm^{-1}, which is high enough for practical applications in electrochemical devices application such as lithium batter-

ies. This value shows greater improvement compared to the classic system, PGMA–LiClO$_4$ without BmimTFSI, which is 2.27×10^{-7} S cm^{-1}. As comparison to the established study carried out by Ramesh et al. [16], our data in solid polymer electrolytes are only one magnitude lower than the highest ionic conductivity achieved by PMMA–PVC blend gel polymer electrolytes with the presence of LiTFSI and BmimTFSI. Recent study by Shalu et al. [33] has found that the incorporation of BmimTFSI in PVdF−HFP + 20 wt % LiTFSI polymeric gel electrolyte membranes has achieved the maximum value of 2×10^{-3} S cm^{-1} at 30°C. PvDF−HFP is known for its strong electron withdrawing and high dielectric constant which is a favorable choice of polymer electrolyte host and has demonstrated sufficient conductivity for commercial usage in secondary batteries [3, 18]. According to Singh et al. [13], the ionic conductivity of SPE depends on the amount and the mobility of the charge carriers. Therefore, the increase in ionic conductivity is mainly due to the increase of the charge carriers in the electrolyte system, as shown by the proportional relationship between the numbers of charges and the ionic conductivity in the following equation,

$$\sigma = ce(u_+ + u_-) = c\lambda, \qquad (3)$$

σ is conductivity, λ is molar conductivity, c is salt concentration, e is charge on an electron, and u_+ and u_- represent the ion mobility [20].

Since ionic liquid comprises of only ions, the addition of ionic liquid into the polymer electrolyte system increases the quantity of charge carriers. Besides, it contributes to the formation of pathway for ionic mobility, hence increases the conductivity values [16]. However, the addition of ionic liquid at more than 60 wt % reduced the ionic conductivity and it is suggested caused by the congested system that limits the ions mobility. It proves that the addition of 70 wt % ionic liquid BmimTFSI reduced the ionic conductivity of the polymer electrolyte to 8.23×10^{-6} S cm^{-1}. However, beyond the maximum value at 60 wt %, the ionic conductivity is expected to decrease along with the film's flexibility from 70 wt % BmimTFSI upward. The maximum ionic conductivity value at 60 wt % BmimTFSI shows the maximum effective interaction between oxygen atoms and the cation in PGMA–LiClO$_4$−BmimTFSI SPE system. The effective interaction can be expressed by the number of interaction between oxygen atoms to the cation or simply written as $[O/Li^+ + Bmim^+]$ ratio. The incorporation of BmimTFSI in PGMA–LiClO$_4$ system is found to increase $[O/(Li^+ + Bmim^+)]$ ratio from [7/1] to [28/1] and subsequently increases the ionic conductivity. This is due to the large number of charge carriers, Li$^+$ ions responsible in increasing the ionic conductivity. The charge carrier weakens the coordination bond between the Li$^+$ with electron withdrawing group, such as (C=O), (C−O−C) and epoxide ring, and pro-
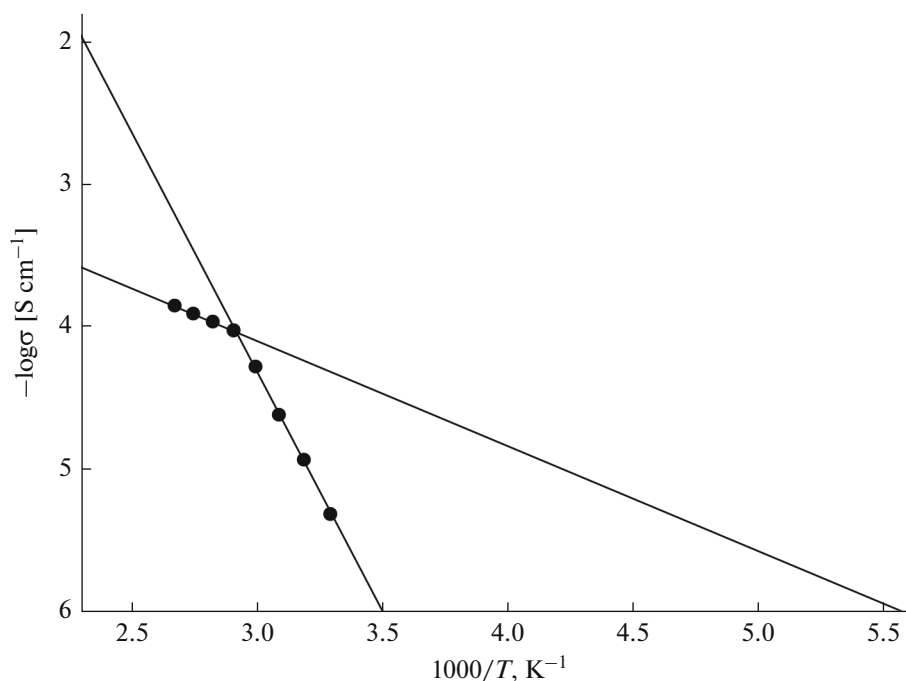
Fig. 7. Arrhenius plots of ionic conductivity for PGMA–LiClO$_4$–60 wt % BmimTFSI SPE.

motes high dissociation rate and ion-migration of [Bmim]$^+$ cation and [TFSI]$^-$ anion. The bulky [TFSI]$^-$ anion structure and low lattice energy confirmation accelerate the ionic dissociation [12]. This helps in decoupling of ion from the polymer backbone and as a result, more mobile carriers are produced and thus, facilitate the ion transportation through the polymer matrix, leading to higher ionic conductivity. As for low concentration of BmimTFSI, the conductivity of the system only depends on the number of charge carriers effectively interacting with polymer host, while the mobility of ion is not counted in this case, on the other hand at higher amount of BmimTFSI, the ionic conductivity is controlled by the ion mobility and formation of ionic conduction pathway [16]. Overall, the effective interaction between the oxygen atoms and the cation in PGMA–LiClO$_4$–BmimTFSI is found to reduce as the BmimTFSI concentration rises from [28/1] to [12/1] of [O/(Li$^+$ + Bmim$^+$)] ratio. The increasing numbers of BmimTFSI conducting species in the PGMA–LiClO$_4$ polymer electrolyte helps to increase the conductivity value [34]. The optimum [O/(Li$^+$ + Bmim$^+$)] ratio for PGMA–LiClO$_4$–BmimTFSI is found at [12/1] for 60 wt % of ionic liquid BmimTFSI with ionic conductivity at 2.56×10^{-5} S cm^{-1}.

Figure 7 demonstrates the temperature dependence plot by two different Arrhenius plots for PGMA–LiClO$_4$–60 wt % BmimTFSI SPE (a) plot 1 for temperature range between 30–70°C, and (b) plot 2 for temperature range between 70–100°C. Plot 1 and plot 2 show linear relationship between conductivity and temperature with the regression line of 0.9989 and 0.9999, respectively. This indicates that PGMA–LiClO$_4$–60 wt % BmimTFSI polymer electrolyte systems exhibit Arrhenius-like behavior at different temperature range. The pre-exponential factor (the maximum ionic conductivity at infinite temperature) of plot 1, $\sigma_0 = 7.05 \times 10^5$ S cm^{-1} is neglected due to deviation from estimated value, whereas the pre-exponential factor of plot 2, $\sigma_0 = 1.40 \times 10^{-2}$ S cm^{-1} is more precise to VTF plot. On the other hand, the activation energy of plot 1, $E_a = 0.15$ eV, indicates low ionic mobility in solid state polymer electrolytes (which is true), and the activation energy from plot 2, $E_a = 0.67$ eV signifies higher ionic mobility after glass transition temperature indicated that the viscosity of the polymer electrolytes decreased. This increases chain flexibility and the segmental motion of the polymer chain, which leads to the increase in the dissociation rate of cation, thus improving the mobility of the carrier charge. As the temperature increases, the viscosity of the polymer electrolytes reduces. This increases the chain flexibility and the segmental motion of the polymer chain, which leads to the rise of free volume, thus improving the mobility of the carrier charge inside the polymer matrix [35]. At high temperature, the ion migration is faster and diminishes the ion cloud effects between the electrode and the electrolyte. The vibrational mode for polymer segment has sufficient energy to push out the hydrostatic pressure from the surrounding atom and turns to the formation of free volume. This free volume promotes the segmental

motion for decoupling process, leading to the formation of empty vacant site, which is available to interact with another cation during ion hopping mechanism and thus, increases ion migration inside the polymer matrix [16].

As noticed by the Arrhenius plots from the experimental data, there is a transition of temperature dependence of conductivity. It follows the Arrhenius behavior at low and high temperatures. This behavior is also observed by Basak and Manorama [36], on the PEO−PU/PAN with LiClO₄, whereby they observed a transition from Arrhenius-like behavior at low temperatures. They suggested that the crossover in temperature dependent conductivity was attributed to the phase morphology change of semi-IPNs above the T_m of the polyether segments. On the case observed by Saibaba et al. [37], above 333 K the conductivity increases abruptly in $PEO-(LiX)_n$ (X: ClO_4,BF_4) polymer electrolytes compared to $MEEP-(LiX)_n$ and $MEEP/PEO-(LiX)_n$. The same observation on $PEO-LiClO_4$ is noticed by Croce et al. [38]. The transition temperatures at 343 K for both plots provide information about the charge carriers and main chain mobility below and above the glass transition temperature (T_g) of PGMA segments. A study by Imperiyka et al. [7] on $PGMA-30$ wt % $LiClO_4$ showed a perfect linear fitting and followed Arrhenius-like behavior, but only up to 343 K and after this temperature, the bulk resistance of polymer electrolyte could not be observed from the impedance spectrum. Therefore, by inclusion of BmimTFSI, the thermal stability range of working SPE is successfully increased up to 373 K. Polymer−LiClO₄ is among the most well studied polymer-salts complexes in classic polymer electrolytes systems and most of them obeyed Arrhenius-like behavior below T_g [7, 39−41]. In addition, this observation may be due to the thermal decomposition of LiClO₄. The first thermal degradation of LiClO₄ salts is reported at 335 K, which is related to the thermal decomposition reaction. The release of the oxygen element from LiClO₄ during the oxygenation process (sometimes could occur even under nitrogen atmosphere), results in an overall exothermic effect [42].

5. CONCLUSIONS

In this work, SPEs were successfully prepared using the solution casting method. The morphological observation shows that the inclusion of BmimTFSI produces smooth and homogenous surface of the electrolyte. The ATR-FTIR and thermal analyses divulge the shift of the spectrum that indicates the complexation between $PGMA-LiClO_4$ and BmimTFSI. The highest ionic conductivity at ambient temperature is 2.56×10^{-5} S cm⁻¹, achieved upon addition of 60 wt % of BmimTFSI due its maximum mobility, and concentration of charge carriers. The systems exhibit Arrhenius-like behavior at two different temperature ranges; low (30−70°C) and high temperatures (70−100°C).

REFERENCES

1. Li, Y., Yerian J.A., Khan, S.A., and Fedkiw, P.S., *J. Power Sources*, 2006, vol. 161, p. 1288.
2. Adebahr, J., Byrne, N., Forsyth, M., MacFarlane, D.R., and Jacobsson, P., *Electrochim. Acta*, 2003, vol. 48, p. 2099.
3. Nicotera, I., Coppola, L., Oliviero, C., Castriota, M., and Cazzanelli, E., *Solid State Ionics*, 2006, vol. 177, p. 581.
4. Ramesh, S., Winie, T., and Arof, A.K., *Eur. Pol. J.*, 2007, vol. 43, p. 1963.
5. Imperiyka, M., Ahmad, A., Hanifah, S.A., and Rahman, M.Y.A., *Int. J. Electrochem. Sci.*, 2013, vol. 8, p. 10932.
6. Hanifah, S.A., Hamzah, N., and Heng, L.Y., *Sains Malaysiana*, 2013, vol. 42, p. 487.
7. Radzir, N.N.M., Sharina, A.H., Ahmad, A., Hassan, N.H., and Bella, F., *J. Solid State Electrochem.*, 2015, vol. 19, p. 3079.
8. Ahmad, A., Rahman, M.Y.A., Su'ait, M.S., and Hamzah, H., *Open Mater. Sci. J.*, 2011, vol. 5, p. 170.
9. Imperiyka, M., Ahmad, A., Hanifah, S.A., Mohamed, N.S., and Rahman, M.Y.A., *Int. J. Hydro. Energy*, 2013, vol. 39, p. 3018.
10. Earle, M.J., Exceranca, S.S., Gilea, A., Lopez, J.N.C., Robelo, L.P.N., Magee, J.W., Seddon, K.R., and Widegren, J.A., *Nature*, 2006, vol. 439, p. 831.
11. Missan, H.P.S., Lalia, B.S., Karan, K., and Maxwell, A., *Mater. Sci. Eng., Ser. B*, 2010, vol. 175, p. 143.
12. Liew, C.W. and Ramesh, S., *Mater. Res. Soc.*, 2012, vol. 23, p. 2996.
13. Singh, P.K., Kim, K.W., and Rhee, H.W., *Synthetic Metals*, 2009, vol. 159, p. 1538.
14. Singh, P.K., Jadhav, N.A., and Mishra, S.K., *Ionics*, 2010, vol. 16, p. 645.
15. Leones, R., Sentanin, F., Rodrigues Luisa, C., Ferreira Rute, A.S., Jose Esperanca, M.S.S., Pawlicka, A., Carlos Luis, D., and Silva Manuela, M., *Opt. Mater.*, 2012, vol. 35, p. 187.
16. Ramesh, S., Liew, C.W., and Ramesh, K., *J. Non-Crystalline Solids*, 2011, vol. 357, p. 2132.
17. Ahmad, A., Lien, P.C., and Su'ait, M.S., *Sains Malaysiana*, 2010, vol. 39, p. 65.
18. Yang, P., Cui, W., Li, L., Liu, L., and An, M., *Solid State Sci.*, 2012, vol. 4, p. 598.
19. Sivakumar, M., Subadevi, R., Rajendran, S., Wu, N.L., and Lee, J.Y., *Chem. Phys.*, 2006, vol. 97, p. 330.

20. Su'ait, M.S., Ahmad, A., Hamzah, H., Noor, S.A.M., and Rahman, M.Y.A., *J. Solid State Electrochem.*, 2012, vol. 16, p. 2275.

21. Hamit, E., Umit, A., and Wolfgang, H.M., *Solid State Ionics*, 2001, vol. 181, p. 1586.

22. Sekhon, S.S., Krishnan, P., Singh, B., Yamada, K., and Kim, K.S., *Electrochim. Acta*, 2006, vol. 52, 1639.

23. Singh, P.K., Kim, K.W., Park, N.G., and Rhee, H.W., *Synthetic Metals*, 2008, vol. 158, p. 590.

24. Shin, J.H., Henderson, W.A., and Passerini, S., *Electrochem. Commun.*, 2003, vol. 5, p. 1016.

25. Jiang, J., Gao, D., Li, Z., and Su, G., *React. Func. Polym.*, 2006, vol. 66, p. 1141.

26. Stephen, A.M., Kumar, T.P., Renganathan, N.G., Pitchumani, S., Thirunakaran, R., and Muniyandi, N., *J. Power Sources*, 2000, vol. 89, p. 81.

27. Liew, C.W., *M. Sc Thesis*, Kuala Lampur University, 2011.

28. Wu, Y., Xiong, L., Qin, X., Wang, Z., Ding, B., Ren, H., and Pi, X., *IOP Conference Series: Materials Science and Engineering*, 2015, vol. 87, p. 012082.

29. Rodrigues, L.C., Barbosa, P.C., Silva, M.M., and Smith, M.J., *Electrochim. Acta*, 2007, vol. 53, p. 1427.

30. Zulfiqar, S., Zulfiqar, M., Nawaz, M., McNeill, I.C., and Gorman, J.G., *Polym. Degradation Stability*, 1990, vol. 30, p. 195.

31. Ahmad, S. and Zulfiqar, S., *Polym. Degradation Stability*, 2002, vol. 76, p. 173.

32. Iqbal, M.S., Jamil, Y., Kausar, T., and Akhtar, M., *J. Therm. Analysis Calorimetry*, 2009, vol. 96, p. 225.

33. Shalu Singh, V.K. and Singh, R.K., *J. Mater. Chem., Ser. C*, 2015, vol. 3, p. 7305.

34. Wang, H.X., Wang, Z.X., Li, H., Meng, Q.B., and Chen, L.Q., *Electrochim. Acta*, 2006, vol. 52, p. 2039.

35. Baskaran, R., Selvasekarapandian, S., Kuwata, N., Kawamura, J., and Hattori, T., *Solid State Ionics*, 2006, vol. 177, p. 2679.

36. Basak, P. and Manorama, S.V., *Solid State Ionics*, 2004, vol. 167, p. 113.

37. Saibaba, G., Srikanth, D., and Reddy, A., *Bull. Mater. Sci.*, 2004, vol. 27, p. 51.

38. Croce, F., Appetecchi, G.B., Persi, L., and Scrosati, B., *Nature*, 1998, vol. 394, p. 456.

39. Tsuchida, E., Ohno, H., and Tsunemi, K., *Electrochim. Acta*, 1983, vol. 28, p. 591.

40. Chen-Yang, Y.W., Chen, H.C., Lin, F.J., and Chen, C.C., *Solid State Ionics*, 2012, vol. 150, p. 327.

41. Choudhary, S. and Sengwa, R.J., *Indian J. Eng. Mater. Sci.*, 2012, vol. 19, p. 245.

42. Lu, Z., Yang, L., and Guo, Y., *J. Power Sources*, 2006, vol. 156, p. 555.